DISSECTING TUMOUR PATHOPHYSIOLOGY USING INTRAVITAL MICROSCOPY

Rakesh K. Jain, Lance L. Munn and Dai Fukumura

For a systemically administered therapeutic agent to reach neoplastic cells, it must enter the blood circulation, cross the vessel wall, move through the extracellular matrix and avoid getting cleared by the lymphatics. In tumours, each of these barriers is abnormal, changes with space and time, and depends on host–tumour interactions. Intravital microscopy has provided unprecedented molecular, cellular, anatomical and functional insights into these barriers and has revealed new approaches to improved detection and treatment.

TRANS-ILLUMINATION
Microscope configuration in which the light passes from the illuminating condenser through the tissue and then into the objective lens. A green filter is often used to increase the contrast of haemoglobin. Applicable only for imaging in relatively thin tissues.

EPI-ILLUMINATION
Microscope configuration in which light comes from the objective lens to the tissue and is then collected by the same objective lens. This is useful for both fluorescent and bright-field (reflectance) microscopy. With the use of appropriate molecular probes and optical filters, specific molecular, cellular, anatomical and functional events can be detected.

Edwin L. Steele Laboratory, Department of Radiation Oncology, Massachusetts General Hospital and Harvard Medical School, Boston, Massachusetts 02114, USA.
e-mail: jain@steele.mgh.harvard.edu
DOI: 10.1038/nrc778

Our investment in cancer research has provided phenomenal insights into the molecular origins of cancer. These insights have led to the identification of many genes that are associated with oncogenesis, as well as a wide array of new therapeutic approaches. The challenge now is to decipher the function of these genes not only *in vitro* or *in silico*, but ultimately in an intact host. A second challenge is to characterize and overcome the physiological barriers to delivery and to improve the efficacy of therapeutic agents in the tumour microenvironment. Intravital microscopy (IVM) has provided powerful insights into gene expression and function in tumours, revealed the crucial role of host–tumour interactions in the biology of tumours and their responses to therapy, and indicated new approaches to improve cancer detection and treatment. So, what is intravital microscopy? And how is it helping us to understand how tumours behave?

Intravital microscopy

Traditionally, we have had two choices for measuring gene expression, physiological and anatomical parameters, and delivery and response to therapy in tumours: we can use invasive techniques that require tissue excision, or non-invasive techniques that have low spatial resolution (mm–cm). The former limit our ability to obtain temporal dynamics, and the latter preclude visualization at the cellular and subcellular levels (1–10 μm). Intravital microscopy can overcome these limitations and provide insights into various molecular and cellular processes *in vivo* with high spatial and temporal resolution down to the subcellular level[1,2].

In its simplest embodiment, quantitative IVM requires four components (FIG. 1): first, a tissue preparation that allows visualization; second, a molecular probe that can be detected by a microscope; third, a microscope and detection system (for example, charged-coupled device camera and computer); and fourth, computer algorithms and mathematical models that can be used to extract parameters of interest from the optical information. In this article, we look at each component.

The tissue preparations fall into three broad categories (TABLE 1; FIG. 1): chronic-transparent windows; acute (exteriorized) tissue preparations; and *in situ* preparations. Each of these preparations can be used to study normal tissue or an implanted tumour. The tumour source can be a suspension of cancer cells or a fragment of tumour tissue. Alternatively, a gel containing defined growth factor(s) or engineered cells can be implanted in these tissue preparations. As with other investigative tools, each preparation has its strengths and weaknesses, and a combination of approaches is normally warranted.

Once the preparation is ready for observation, the animal is brought to the stage of a specially designed microscope (FIG. 1). Depending on the experimental aim, an appropriate exogenous or endogenous molecular probe is used (TABLE 2), and

Summary

- A solid tumour is an organ-like structure that consists of cancer cells and host stromal cells embedded in an extracellular matrix and nourished by a vascular network. Intravital microscopy (IVM) has provided unprecedented molecular, anatomical and functional insights into the inner workings of this organ and provided a means for testing the efficacy of various therapies.
- IVM is a powerful optical imaging technique that allows continuous non-invasive monitoring of molecular and cellular processes in intact living tissue with 1–10 μm resolution. Such resolution is currently not possible with non-optical techniques.
- IVM requires an appropriate animal model, a molecular probe (usually fluorescent), a microscope equipped with a digital camera detection system, an image acquisition system, and a computer to process and analyse the data to extract parameters of interest.
- Molecular imaging has revealed heterogeneity in the tumour microenvironment (for example, pO_2 and pH) and the delivery of therapeutics (micro-pharmacokinetics). The most celebrated applications of molecular imaging include measurement of promoter activity, enzyme activity and gene expression *in vivo*.
- Cellular imaging has uncovered key steps in the spread of cancer from one site to the next (invasion and metastasis), and barriers to various cell-based therapies (for example, immunotherapy and gene therapy). Cellular imaging has also allowed measurement of interactions among various subpopulations of cells in a tumour.
- Anatomical imaging has allowed quantification of morphological abnormalities in tumour vessels, as well as the size of pores in their walls.
- Functional imaging has revealed that tumour blood flow, vascular permeability, interstitial diffusion, convection and binding are spatially and temporally heterogeneous in tumours, depend on the host–tumour interactions, and change during the course of treatment. Functional lymphatics are present only in the tumour margin and the peri-tumour tissue.
- IVM has revealed that certain direct and indirect anti-angiogenic treatments can 'normalize' the abnormal tumour vessels so that they become more efficient. This finding underscores the importance of optimal dose and scheduling in combination therapy.
- With the availability of hand-held microscopes and safe (Food and Drug Administration approved) molecular probes, IVM has the potential to become a useful clinical tool to monitor integrative pathophysiology and the response of optically accessible tumours to various therapies in cancer patients.

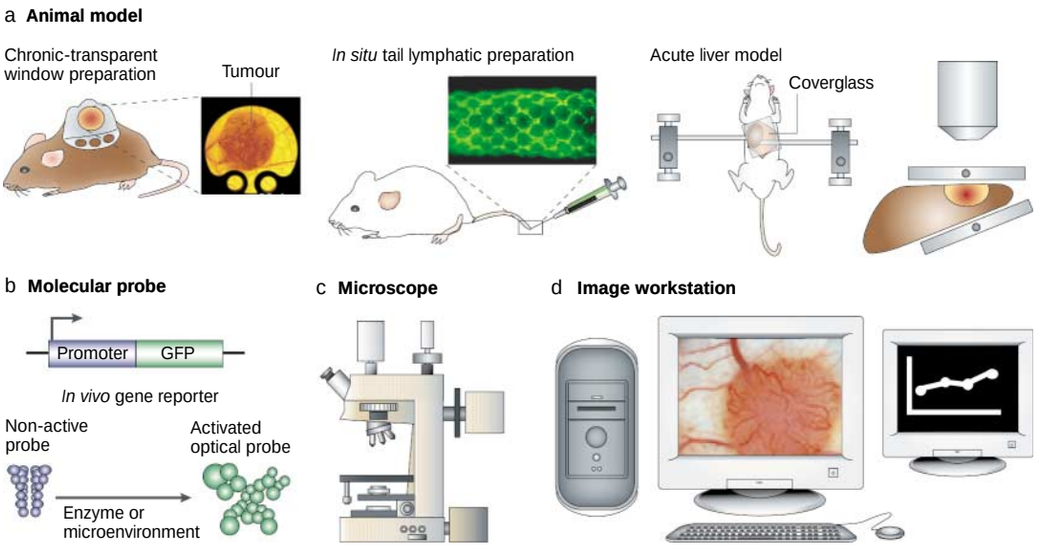

Figure 1 | **Four requirements for intravital microscopy. a** | An appropriate animal model. Three different models are shown: a chronic-transparent window in which a tumour grown on the inner surface of the skin can be viewed through a coverslip; an *in situ* preparation in which an optical tracer is injected into the interstitial space of the tail; and an acute liver model in which the animal is surgically prepared to reveal a tumour in the internal organ. **b** | A molecular probe (usually fluorescent) that can be imaged. Two examples are shown: green fluorescent protein (GFP) that is expressed in genetically engineered cells/animals and controlled by the promoter of interest; and an optical probe that is activated by a specific enzyme or microenvironment. **c** | A microscope equipped with an excitation source and a detection system (such as photomultiplier tube (PMT) or charged-coupled device/silicon-intensified target (SIT) camera), which passes the images to a computer acquisition and analysis work station. **d** | Image processing and analysis algorithms are then applied to extract quantitative data. Part **a** (left) adapted with permission from REF. 66 © (1992) American Association for Cancer Research; part **a** (middle) adapted with permission from REF.59 © (2000) American Association for Cancer Research.

Table 1 | Examples of various intravital preparations for tumour studies

Models	Species	Tumour	Year	References
Chronic-window preparations				
Ear chamber	Rabbit	Rabbit CA Rabbit CA: intra-arterial injection Rabbit CA: multifocal growth	1939 1958 1984	108 25 5,109
Dorsal skin chamber	Mouse	Various CAs, SAs, melanomas Hepatoma 134 Mammary CA	1943 1961 1971	110,111 112 113
	Nude mouse	Human amelanotic melanoma	1984	114
	SCID mouse	Human tumour xenograft	1992	66
	Hamster	Amelanotic melanoma	1981	115
	Rat	Ascites hepatoma Rhabdomyosarcoma Rat SA Rat mammary CA	1971 1977 1979 1989	116 117 53,54 118
Cranial window	Rat and mouse	Various rodent and human tumours	1994	6
Acute (exteriorized) preparations				
Cheek pouch	Hamster	Chemically induced SAs Human tumours Melanomas, CA, human angiopericytoma Malignant neurilemmoma	1950 1952 1965 1973	119 120,121 122 123
Mesentery	Rabbit	Rabbit CA: intra-arterial injection	1961	26
	Rat	Mouse colon CA	1990	124,125
Cremaster muscle	Rat	Rat CA, chondrosarcoma	1986	126
Liver	Mouse	Human adenocarcinoma	1997	39
Mammary gland	Mouse	Human mammary CA	1998	127
Pancreas	Mouse	Human pancreatic CA	1999	128,129
Lung	Mouse	Lewis lung CA	2000	130
In situ preparations				
Eye anterior chamber	Frog	Renal CA	1939	131
	Guinea pig	Human tumour	1952	132
Anterior chamber/ iris assays	Rabbit	Mouse mammary tumour Mouse mammary papilloma Hyperplastic rat mammary gland	1976 1977 1977	133 134 135
Corneal micropocket assay	Rabbit	Rabbit CA, VX2 CA	1974	136,137
	Mouse	Mouse mammary CA and SA	1979	138
Ear	Mouse	Mouse mammary CA	1963	139
Tail lymphatics	Mouse	Mouse fibrosarcoma	2000	59
Specialized models				
Individual microvessel perfusion	Mouse	Human adenocarcinoma	1996	70
Angiogenesis gel assay	Mouse	Various angiogenesis factors	1996	140

CA, carcinoma; SA, sarcoma; SCID, severe combined immunodeficiency. Adapted from REF. 2.

CONFOCAL LASER-SCANNING MICROSCOPE (CLSM). A high spatial-resolution fluorescence microscope that uses scanning laser light for excitation and a pinhole in the emission light path that detects a signal only from the focal plane. CLSMs can provide ~1-μm three-dimensional resolution.

MULTI-PHOTON LASER-SCANNING MICROSCOPE (MPLSM). A high spatial-resolution fluorescence microscope using low energy (long wavelength) photons that are produced by an infrared laser. Multi-photon excitation occurs only in a small volume in which the photons are focused. The long-wavelength photons and high signal-to-noise ratio allow subsurface imaging (~700 μm) with ~1-μm three-dimensional resolution, minimal photo-damage and longer probe lifetimes in thick samples.

either TRANS-ILLUMINATION or EPI-ILLUMINATION is applied to visualize the whole tissue (for example, mesentery) or only the superficial regions (for example, cranial window). The optimal type of illumination is dictated by the thickness of the tissue and its optical properties.

Increasing depth of imaging can be achieved by CONFOCAL LASER-SCANNING MICROSCOPES (CSLMs) and MULTI-PHOTON LASER-SCANNING MICROSCOPES (MPLSMs). The latter offer significant advancements, such as improved signal-to-noise ratio, imaging depth of up to 700 μm, minimal photo-damage and longer probe lifetimes in thick samples[3,4].

A historical perspective, descriptions of the surgical procedures for making various tissue preparations, details of constructing intravital microscopes for different purposes, as well as the computer-assisted analyses/techniques that are used to extract parameters of interest from images acquired via intravital microscopy, can be found in references in TABLES 1 and 2, as well as in two review articles[1,2].

Molecular imaging

In principle, any molecule that can be detected by optical microscopy can be tracked by molecular

Table 2 | Examples of parameters measured and probes used in IVM

Parameter	Molecular probe	References
Molecular imaging		
Micro-pharmacokinetics	FITC-antibody, TMR-liposome	51,76
Microenvironment (pH, pO_2)	BCECF, BSA–porphyrin	8–10,141
Enzyme activity (cathepsin B, protein kinase A, tyrosine kinase)	NIRF probe-graft copolymer, CFP–14-3-3τ–YFP reporter gene	12,14,15
Gene expression	GFP reporter gene	97
Promoter activity	VEGFp–GFP	11,16
Cellular imaging		
Tracking cancer cells	GFP, calcein, fluorescent nanosphere	27–32,91
Tracking leukocytes	Rhodamine 6G, calcein	3,34–37
Tracking other cells	GFP	3
Anatomical imaging		
Tumour size	Endogenous contrast, GFP	66,91
Vascular architecture (diameter, length, surface area, volume, branching patterns)	Endogenous contrast, OPS, FITC/TMR–dextran	50–52,66
Lymphatic architecture (diameter, length, branching patterns)	FITC/TMR–dextran	4,60,79,80
Pore size	TMR-liposome/microsphere with varying size	62,63
Functional imaging		
Blood-flow rate	FITC–dextran, endogenous contrast	3,53,54,66,142
Lymph-flow rate	FITC–dextran	80,81
Vascular permeability	TMR/Cy5–BSA	3,68–70
Interstitial diffusion, convection and binding	Fluorescent BSA, IgG, dextran, microsphere, liposome	75–78

BCECF, 2′,7′-bis-(2-carboxyethyl)-5,6-carboxyfluorescein; BSA, bovine serum albumin; CFP, cyan fluorescent protein; FITC, fluorescein isothiocyanate; GFP, green fluorescent protein; Ig, immunoglobulin G; NIRF, near-infrared fluorescence; OPS, orthogonal polarization spectral; 14-3-3τ, phosphoamino-acid-binding domain; porphyrin, palladium meso-tetra (4-carboxyphenyl) porphyrin; TMR, tetremethylrhodamine; VEGFp, vascular endothelial growth factor promoter; YFP, yellow fluorescent protein.

imaging *in vivo*. The easiest, and hence most widely used, application of this concept is monitoring the delivery (micro-pharmacokinetics) of molecularly targeted therapeutics (FIG. 2a). The therapeutic agent can be naturally fluorescent (for example, adriamycin) or tagged with a fluorescent tracer; for example, therapeutic antibodies can be tagged with fluorescein isothiocyanate (FITC). If the agent is delivered using a carrier, such as a liposome, then both the drug and the carrier can be monitored using different optical tracers. Such an approach led us to the conclusion that it is difficult to deliver therapeutic agents in optimal quantities to all regions of a tumour[5,6], and this spawned our interest in understanding physiological barriers to drug delivery[7].

Monitoring molecules that are present in a tissue, but not naturally fluorescent, requires molecular probes that change their optical properties as a function of the concentration of the test molecule and independently of the concentration of the probe (FIG. 2b). Molecular probes that respond optically to changes in pH and pO_2 have been successfully used to map the metabolic microenvironment of tumours[8,9]. These studies have shown that tumours can contain hypoxic regions, despite active blood flow. Moreover, low pH and low pO_2 can be independent of each other[10]. This finding has significant implications for the efficacy of drugs and/or expression of genes that respond to low pH or hypoxia[11].

Similarly, monitoring the activity of an enzyme requires a molecular probe that changes its optical properties by specific interaction with the enzyme (FIG. 1b). As the product of the reaction accumulates in the tissue, the optical signal increases (or, in some cases, decreases) in proportion to the enzyme activity. Such an approach has been successfully applied to monitor the activity of cathepsin B using near-infrared (NIR) imaging[12] and epi-fluorescence microscopy (D. Fukumura *et al.*, unpublished observations). This area of molecular imaging is awaiting the development of new molecular probes to monitor different enzymes[12,13] and receptors[12,13] that are involved in tumour progression, and to assess their involvement in different signalling pathways[14,15].

Finally, the most exciting and innovative area of molecular imaging provides a tool for monitoring gene expression and regulation *in vivo*. The recent discovery and commercial availability of live fluorescent reporters such as green, blue, cyan, yellow, red and far-red fluorescent proteins (GFP, BFP, CFP, YFP, DsRed and HcRed, respectively) have made this feasible. By creating transgenic cell lines or animals that express GFP or its spectral variants under the control of the promoter of the gene of interest, it is now possible to monitor promoter activity as well as the parameters of the microenvironment that regulate this activity[11,16]. Such an approach has revealed that cancer cells can activate stromal cells to produce vascular endothelial growth factor (VEGF), a potent angiogenic molecule[16] (FIG. 2c,d), and that stromal cells actually produce up to 50% of the total VEGF in a tumour[17]. The stromal cells can also affect the production of endogenous inhibitors of angiogenesis and influence distal metastases[18]. These discoveries underscored the importance of host–tumour interaction in tumour angiogenesis, growth and metastasis[19,20].

Because the stromal cells in each organ are different, the biology of a tumour is likely to depend on the organ in which it resides. Furthermore, within a given organ the heterogeneity in the metabolic microenvironment will lead to heterogeneous expression of genes[11]. It is easy to imagine that live reporters can also be useful for monitoring the delivery of therapeutic genes via viral or non-viral vectors. Furthermore, by using different variants of GFP and luciferase[21] it should be possible to monitor the expression of, and the interactions among, several genes and their products simultaneously. With the availability of live reporters that change 'colour' (wavelength of peak emission) with time[22,23], under different conditions (for example, in the presence or absence of a particular signalling molecule[14,15]) or when activated by a laser[24], it should be possible to determine the time course of gene-expression and signal-transduction pathways *in vivo*.

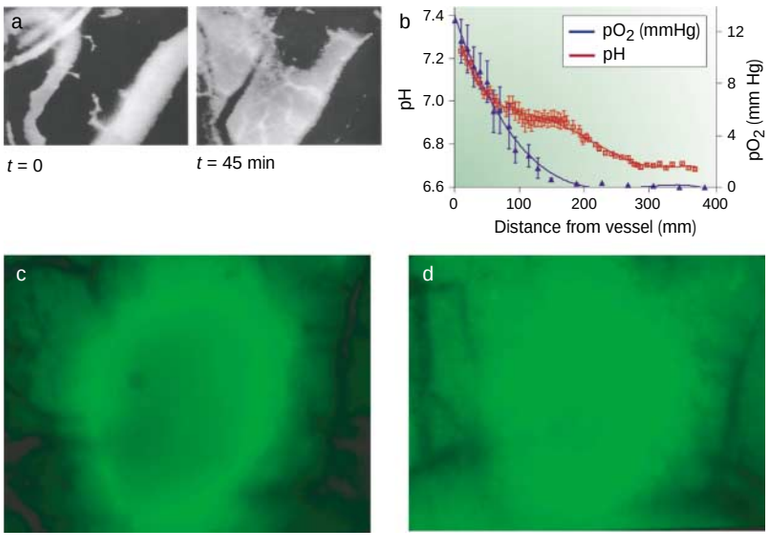

Figure 2 | **Molecular imaging.** The accumulation of fluorescent molecules in various tissues can be quantified through changes in fluorescent intensity over time. **a** | Extravasation of fluorescein isothiocyanate (FITC)–dextran tracer out of a blood vessel provides a measure of micro-pharmacokinetics; **b** | pH (red) and pO_2 (blue) profiles as a function of distance from a blood vessel inside the tumour can be measured optically and non-invasively using ratio imaging and phosphorescence quenching, respectively; **c**,**d** | gene expression is tracked *in vivo* using intravital reporters such as green fluorescent protein (GFP). In this case, expression of GFP indicates activation of the promoter for vascular endothelial growth factor in stromal cells, initially at the periphery of the tumour (**c**, 1 week after implantation), and eventually throughout the tumour (**d**, 2 weeks after implantation). Part **b** adapted with permission from REF. 10 © (1997) Macmillan Magazines Ltd; and parts **c** and **d** reproduced with permission from REF. 16 © (1998) Elsevier Science.

Cellular imaging

Intravital microscopy has provided powerful insights into cell–cell interactions *in vivo*, and especially in the movement of cancer cells (FIG. 3a) and cells of the immune system (FIG. 3b) — the former to understand various steps in metastasis and the latter to improve immunotherapy of cancer. In a series of seminal studies in the 1950s and 1960s, respectively, Wood and Zeidman tracked the movement of neoplastic cells injected intra-arterially into the rabbit ear chamber[25] and the rabbit mesentery[26]. They discovered that, owing to their size and mechanical rigidity, cancer cells get stuck at the arterial side of the capillary network, but they extravasate on the venous side of the network. In the 1990s, Chambers, Groom and colleagues, using various cytoplasmic and membrane dyes, tracked the movement of cancer cells in the liver and other organs, and proposed that extravasation at the target organs is not the rate-limiting step in metastasis[27]. Recently, a number of investigators have used cells that constitutively express GFP in combination with video-microscopy to monitor various steps of tumour growth, angiogenesis and metastasis. The key findings from these studies include the following. First, implanted tumour cells migrate towards host blood vessels before their proliferation and induction of angiogenesis[28]; second, the lining of tumour blood vessels has non-uniform expression of endothelial markers (such as CD31 and CD105), and has therefore been dubbed 'mosaic' vessel[29]; third, tumour cells migrate, intravasate and are carried to a secondary site at a rate that is proportional to the metastatic potential[30]; and fourth, cells lodged in the secondary site frequently stay dormant[31,32]. Unfortunately, IVM has not been applied to discern the various steps of lymphatic metastasis, presumably owing to a lack of suitable animal models[33]. With the availability of engineered cancer cell lines and mice that overexpress or lack the genes that encode molecules involved in metastasis, IVM will continue to provide new insights into metastasis.

Using IVM, we and others have shown that rolling of endogenous leukocytes is generally low and heterogeneous in tumour vessels, whereas stable adhesion is comparable between normal and tumour vessels[34–40]. We have also examined the adhesion kinetics of exogenously injected activated lymphocytes in normal and tumour vessels, and found that these cells adhere to some tumour vessels and not others[41,42]. Might this heterogeneous adhesion reflect heterogeneous expression of adhesion molecules on these vessels? In our efforts to understand the origins of the heterogeneous expression of adhesion molecules, we discovered that VEGF upregulates various adhesion molecules (such as ICAM1, VCAM1 and E-selectin), whereas basic fibroblast growth factor (bFGF), another potent angiogenic stimulator, downregulates these adhesion molecules[43]. This unexpected connection between angiogenesis (VEGF) and inflammation (leukocyte adhesion) has been confirmed in a number of *in vivo* models[17,44,45], and has been proposed to be mediated by the VEGF receptor 1 (VEGFR1)[46]. This upregulation of adhesion molecules could not be detected using immunostaining[44], and highlights the power of IVM. IVM also showed the role of red blood cells (RBCs)[47] and the age of the animal in leukocyte–endothelial interaction[48]. With the availability of engineered mice that overexpress or lack the genes of relevant molecules, IVM will continue to help unravel the mystery of the immune system, and provide insights into how we might exploit it for cancer treatment[37,40].

MPLSMs have provided new insights into the role of other host cells (for example, fibroblasts, endothelial precursor cells and embryonic stem cells) in tumour growth and angiogenesis. For example, by growing tumours in VEGF–GFP transgenic mice, we have tracked the movement of activated host stromal cells and discovered that these cells wrap around the angiogenic vessels, and that they might even guide the formation of angiogenic vessels in tumours[3] (FIG. 3c). Similarly, by growing a benign tumour from a mixture of cells in which 50% were wild type for hypoxia-inducible factor-1α (HIF1α, an important transcription factor in the response to hypoxia) and 50% were *HIF1α*$^{-/-}$ and also expressed GFP, we have shown that *HIF1α*$^{-/-}$ cells tend to localize to hypoxic regions of the tumour[3] (FIG. 3d). Finally, by grafting the bone marrow from a GFP mouse or injecting a defined population of GFP-expressing cells (for example, endothelial precursor cells), we can track their movement, incorporation and proliferation in

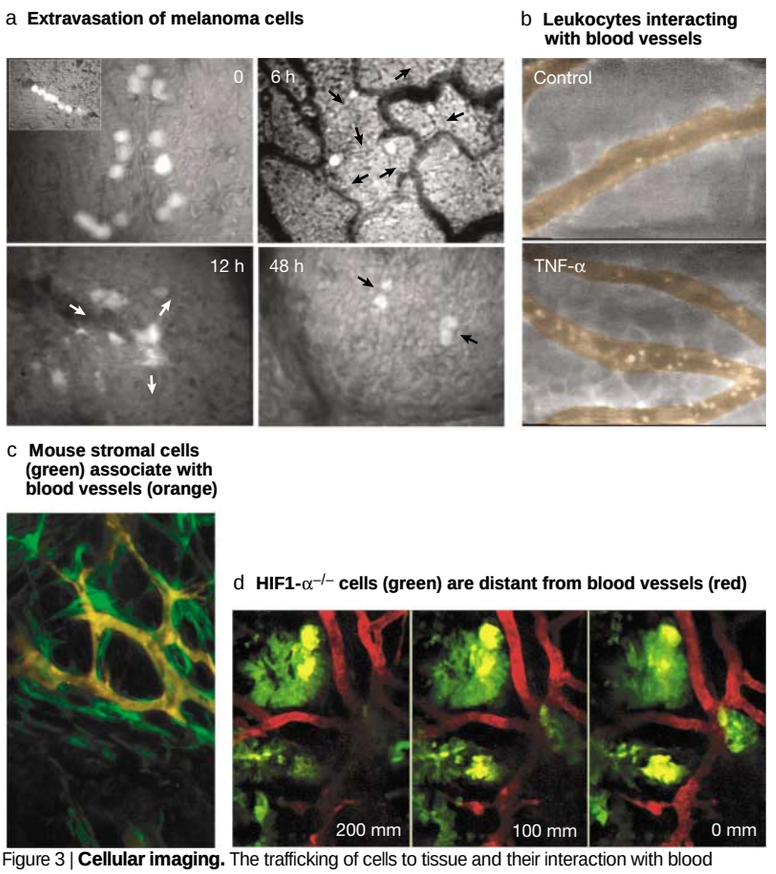

Figure 3 | **Cellular imaging.** The trafficking of cells to tissue and their interaction with blood vessels can be assessed using intravital microscopy. **a** | Ten minutes after systemic injection, fluorescent melanoma cells arrest near the connection of arterioles to the capillary plexus by size restriction. Some cells form rows in capillary segments, because they cannot pass an initially arrested cell (inset). Six hours after injection, cells are still round, and blockage of numerous capillaries (arrows) results in an overall decrease in blood-flow rate. Twelve hours after injection, the cells spread, and are still associated with capillaries or arterioles (arrows indicate flow direction). Forty-eight hours after injection, cell doublets are observed in the parenchyma. **b** | Increase in adhesion of rhodamine-6G-labelled leukocytes with blood vessels after treatment with tumour-necrosis factor-α (TNF-α). **c** | Fortification of the vessel wall with pericytes can be tracked if they express fluorescent reporter constructs. Here, GFP-producing stromal cells organize around the vascular network (orange, rhodamine–dextran). **d** | Using ectopic green fluorescent protein (GFP) expression, cells lacking hypoxia-inducible factor-1α (HIF1-α) expression (green, GFP) can be located in relation to blood vessels (red, rhodamine–dextran) non-invasively. The three panels represent various depths in the tissue. Part **a** reproduced with permission from REF. 106 © (1997) American Society for Investigative Pathology; parts **c** and **d** reproduced with permission from REF. 3 © (2001) Macmillan Magazines Ltd.

tumours (G. D. Duda *et al.*, unpublished observations). Although various invasive techniques[49] can provide similar spatial information, they miss the temporal dynamics that are provided by IVM. So, IVM can be used to increase our understanding not only of tumour biology, but also of developmental biology, regenerative medicine and tissue engineering.

Anatomical imaging

Determining the size and architecture of a tumour and its vasculature is perhaps the most common application of IVM. In general, vessel diameter, length, intercapillary distance and branching patterns can be determined using RBCs as a natural contrast agent under conventional transillumination or linearly polarized light[50]. Alternatively, a high-molecular-weight fluorescent tracer (for example, FITC-conjugated 2-MDa dextran) can be used to demarcate the blood vessels before it begins to leak appreciably into the extravascular compartment (FIG. 4a). It is straightforward to calculate the vascular surface area and volume of a growing or regressing tumour using these parameters and stereological principles[51,52]. A striking finding from such studies is that tumour vessels have an abnormal morphology: they are dilated, saccular, tortuous and have abnormal branching patterns[53–55] (FIG. 4a). FRACTAL ANALYSIS of normal and tumour vascular networks reveals that the former are optimally designed to provide nutrients by diffusion to all normal cells (so-called diffusion-limited aggregation), whereas the latter are restricted by the mechanical properties of the matrix (called invasion percolation)[56,57]. Interestingly, during the course of various direct and indirect anti-angiogenic therapies, tumour vessels begin to develop a normal appearance: their diameter begins to decrease, they become straighter and less tortuous, and their fractal dimension begins to decrease towards the diffusion-limited aggregation pattern[45,46,52,57,58]. We will discuss later the implication of these findings for optimizing combination therapy.

IVM has also provided powerful insights into the pathophysiology of lymphatics in and around tumours. Fluorescence MICRO-LYMPHANGIOGRAPHY (FIG. 4b) of tumours growing in the tails of mice has shown that the lymphatics in the tumour margin are hyperplasic, similar to those in the skin of mice that are engineered to overexpress VEGFC — a growth factor believed to be involved in lymphangiogenesis — in their keratinocytes[59–61]. The diameters of these lymphatics in the tumour margin increase even further in tumours that overexpress VEGFC[33,60]. Surprisingly, overexpression of VEGFC does not induce any functional lymphatics within these tumours. The lack of functional lymphatics within tumours is a key contributor to the interstitial hypertension that is measured in animal and human tumours[7,33].

Owing to physical limitations of optical microscopy, it is not possible to directly measure the dimensions of submicron structures *in vivo*. However, such measurements can be made by monitoring the movement of submicron particles in the tissue (FIG. 4c). For example, by titrating the extravasation of fluorescent nano-particles of increasing size, we found that the cut-off size of 'pores' in the walls of tumour vessels is dependent on the tumour type, the location of its growth and whether it is growing or regressing[62,63]. This PORE CUT-OFF SIZE varied from ~100 nm to 2 μm depending on the tumour. Furthermore, we found that the pore size was dependent on the organ in which the tumour was grown[62]. This pore dimension, which was later confirmed by electron microscopy[64], indicated that widened interendothelial junctions, instead of the transcellular pores, represent the main pathways for macromolecular transport in these tumours. In a testosterone-dependent tumour model, the pore cut-off size decreased following castration, which led to downregulation of VEGF[62]. This approach of relating structure to function is likely to provide new insights into the molecular determinants of VASCULAR PERMEABILITY in tumours.

FRACTAL ANALYSIS
A mathematical analysis for characterizing complex, repeating geometrical patterns at various scale lengths.

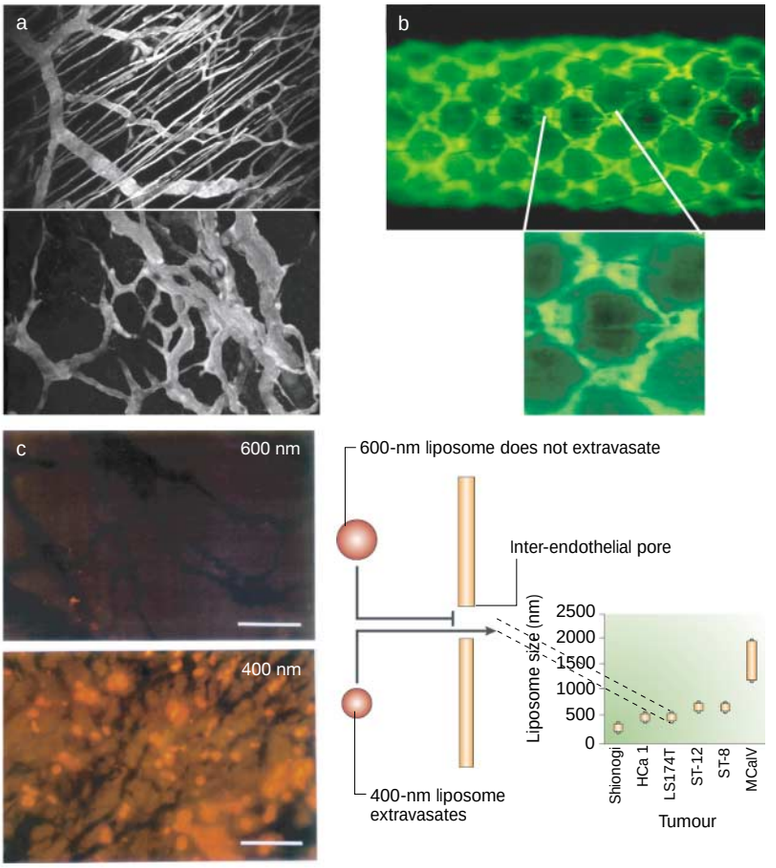

Figure 4 | **Anatomical imaging. a** | Well-organized normal vasculature (top) and chaotic, abnormal tumour network (bottom) in various animal models can be studied for extended periods. **b** | Lymphatic vessels in the tail are easily visualized by lymphangiography. Measurements include vessel diameters, lengths and branching patterns. **c** | Inter-endothelial pore size, measured by titrating extravasating bead size. In this example, 600-nm liposomes do not extravasate, but 400-nm liposomes do, indicating that the pore cut-off size for this tumour lies in the range 400–600 nm. The plot shows that different tumours have different pore sizes. Part **a** courtesy of Edward Brown, Massachusetts General Hospital; part **b** reproduced with permission from REF. 59 © (2000) American Association for Cancer Research; part **c** (left) adapted with permission from REF. 107 © (1997) Macmillan Magazines Ltd.; and part **c** (right) adapted with permission from REF. 62 © (1998) National Academy of Sciences USA.

MICRO-LYMPHANGIOGRAPHY
An imaging technique to visualize functional lymphatic micro-vessels *in vivo*. Locally injected fluorescent macromolecules (such as fluorescein-isothiocyanate-conjugated dextran) are taken up by the lymphatics and can be visualized by intravital microscopy.

PORE CUT-OFF SIZE
Maximum size of particle that can cross the blood-vessel wall. In general, tumour vessels have a significantly larger pore cut-off size compared with their normal counterparts. Pore size depends on the host–tumour interactions and can change during tumour growth and response to therapy.

Functional (physiological) imaging

IVM has enriched our understanding of the various physiological determinants of drug delivery to tumours. A blood-borne agent must be delivered via the vasculature, enter the tissue by transvascular exchange, move through the interstitial space by diffusion or convection, and be cleared by lymphatics in the tumour margin[7,65].

Beginning with the seminal work of Intaglietta and co-workers[53,54], several groups have shown that blood perfusion in tumours is spatially and temporally heterogeneous[3,6,36,38,39,55,66]. Furthermore, in some tumours, average RBC velocity is lower than that in host vessels and does not correlate with vessel diameter[3,6,66] (FIG. 5a). The heterogeneous and chaotic microcirculation of tumours results, in part, from the abnormal architecture of the vascular network, and adversely affects both the delivery of drugs and the metabolic microenvironment. The latter, in turn, compromises the effectiveness of various therapies, and selects for more aggressive and metastatic cancer cells[67].

Measuring the permeability of the tumour vascular network as a whole[62,68,69], as well as of individual tumour vessels[3,70] (FIG. 5b), has revealed it to be an order of magnitude higher than that of most normal vessels. Some gliomas, however, have a low vascular permeability resembling that of the blood–brain barrier, probably due to the lack of placental growth factor (PlGF), a member of the VEGF family[6,71]. The large pore size that is characteristic of most tumour vessels means that they lack selectivity for the size of extravasating molecules[72]. Nevertheless, the permeability and vascular accumulation of cationic macromolecules is higher than that of anionic molecules[73], probably because of the negative charge of angiogenic vessels[74]. Vascular permeability of different tumours growing in the same site is different[6], and varies as the same tumour is grown in different sites[39] or as it responds to therapy[45,46,52,58]. Although it is possible to lower the vascular permeability of a tumour by blocking VEGF signalling[46,52], increasing permeability by adding VEGF or PlGF is not always possible[63]. But perhaps the biggest challenge in transvascular transport in tumours stems from the spatial and temporal heterogeneity in permeability[63,72], which restricts access to some regions of tumours.

Even after a drug molecule has overcome these barriers to extravasation, it must negotiate the extracellular matrix to reach cancer cells. By adapting FLUORESCENCE RECOVERY AFTER PHOTOBLEACHING (FRAP) methodology to intravital applications (FIG. 5c), we have measured the interstitial diffusion, convection and binding of macromolecules in tumours *in vivo*[75,76]. These studies have shown that diffusive transport of macromolecules is slower in tumours than in water, and that it decreases with molecular weight and binding affinity[75–77]. Furthermore, collagen content and structure is the key determinant of interstitial diffusion in tumours; glycosaminoglycans are not as important[77]. As collagen is mostly produced by the host cells, and the host cells vary from one organ to the next, the diffusion coefficient in tumours is host-organ dependent[78]. Moreover, downregulating collagen synthesis or upregulating collagenase production might serve as a potential strategy for improving delivery of molecular therapeutics (T. McGee *et al.*, unpublished observations).

In most normal tissues, excess fluid and macromolecules are reabsorbed by the lymphatic capillaries (FIG. 5d) and brought back to the thoracic duct. Using two different intravital methods, fluid velocity in the lymphatic capillaries was ~1 to 10 μm/s — considerably faster than the interstitial fluid velocity (~ 0.1 μm/s), but slower than blood velocity (~ 100–1000 μm/s)[79–81]. Surprisingly, hyperplasic lymphatics in the mouse skin induced by overexpression of VEGFC had impaired flow[61]. As stated in the previous section, we were unable to detect any functional lymphatics within tumours with normal or elevated levels of VEGFC[33,59,60]. We propose that the hyperplasic lymphatics that are present in the margin of these tumours are adequate for carrying cancer cells to the

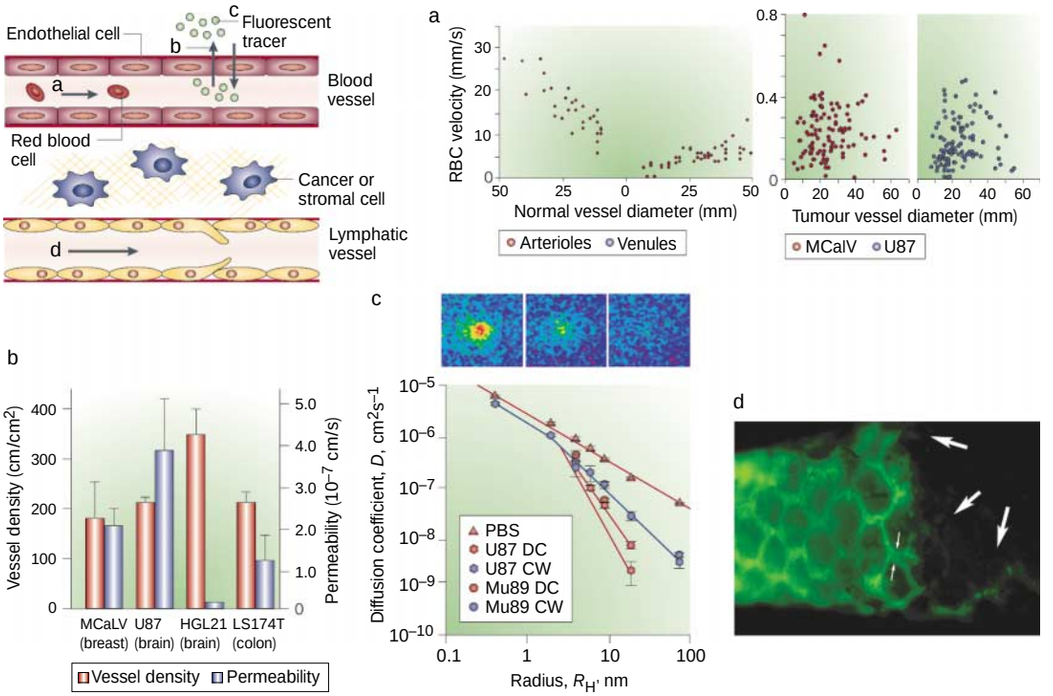

Figure 5 | **Functional imaging.** Intravital microscopy has provided insight into all four barriers to delivery in tumours. **a** | Abnormalities in tumour blood flow (that is, red-blood-cell velocity, V_{max}) quantified using intravital microscopy; in the normal vasculature, velocity is higher in arterial vessels than in venous vessels, and decreases with vessel size. In tumour blood vessels, these relationships do not exist. **b** | Vascular permeability measured by the extravasation of a fluorescent tracer. Permeability and angiogenesis do not correlate in four different tumours in the same site. **c** | Movement of a fluorescent tracer into a photobleached spot (top) gives diffusion coefficients in two tumour types in two locations *in vivo* (bottom). Data from various tumour types (bottom) help design appropriate therapeutic regimens. **d** | By injecting fluorescent tracer subcutaneously, it is possible to observe flow in lymphatic networks. Flow in the network is interrupted by an implanted tumour (large arrows). The small arrows indicate dilated peritumour lymphatics. Part **a** reproduced from REF. 6; part **b** reproduced with permission from REF. 71 © (2000) Macmillan Magazines Ltd; part **c** (top) reproduced with permission from REF. 107 © (1997) Macmillan Magazines Ltd.; part **c** (bottom) reproduced with permission from REF. 78 © (2001) National Academy of Sciences USA; and part **d** reproduced with permission from REF. 59 © (2001) American Association for Cancer Research.

VASCULAR PERMEABILITY
A measure of the propensity of a molecule to extravasate from the vessel lumen to the tissue. Transport of systemically injected tracers, such as tetramethyl-rhodamine-labelled albumin, is monitored by intravital microscopy to estimate vascular permeability. Tumour vessels generally have high vascular permeability.

FLUORESCENCE RECOVERY AFTER PHOTOBLEACHING (FRAP). An imaging technique to measure diffusion, convection and binding of fluorescent molecules. First, tissues are loaded with fluorescent molecules (typically fluorescein isothiocyanate labelled); strong laser light bleaches a pattern in the tissue and the recovery of fluorescence in the bleached pattern is monitored. The rate of recovery is proportional to diffusivity of the molecules in the tissue.

nearby lymph node. Intravital studies of cell movement in these peritumour lymphatics are needed to test this hypothesis[33].

Imaging therapeutic response

In general, the preclinical response to a new therapy is quantified in terms of reduction in (or stabilization of) tumour size and survival time of the animal. However, the ability to monitor several parameters simultaneously with IVM has provided integrated insight into a tumour's response to various therapies. This insight has led to new strategies for improving cancer detection and treatment. For example, we have recently shown that blocking VEGF or VEGF receptor 2 (VEGFR2) leads to a decrease in vessel diameter and vessel density (anatomical imaging) and a decrease in vascular permeability (functional imaging)[17,46,52]. This 'normalization' of tumour vessels can lower interstitial fluid pressure, improve perfusion and, in some cases, increase tissue pO_2 (molecular imaging) (REFS 46,82,83). Similar normalization has been observed intravitally following hormone withdrawal from a testosterone-dependent tumour[45] (FIG. 6a) and following treatment of an ERBB2 (also known as HER2/*neu*)-overexpressing tumour with trastuzumab (Herceptin) — a monoclonal antibody to ERBB2 (REF. 58). This indicates that a cytotoxic therapy (such as radiation or chemotherapy) applied during this 'normalization' window might lead to synergistic effects[84] (FIG. 6b). Indeed, this hypothesis is supported by the successful outcome of combined treatment with a cytotoxic and an anti-angiogenic agent, TNP-470 (REFS 85,86). Conversely, if vessels are obliterated to the point that the microcirculation is compromised, the combination might lead to antagonistic results. This has happened in the cases in which TNP-470 was combined with radiation therapy[87] and chemotherapy[88]. These examples underscore the importance of optimal dosing and scheduling in combination therapy that is based on functional *in vivo* imaging. The challenge is to develop imaging technology for clinical use that can provide molecular, anatomical and functional data with the same temporal and spatial resolution as animal-model imaging.

Future directions

IVM has provided useful insights into many aspects of tumour biology[7,27,65,67,89–91]. However, there are several unanswered questions awaiting the development of new animal models, probes and microscopes.

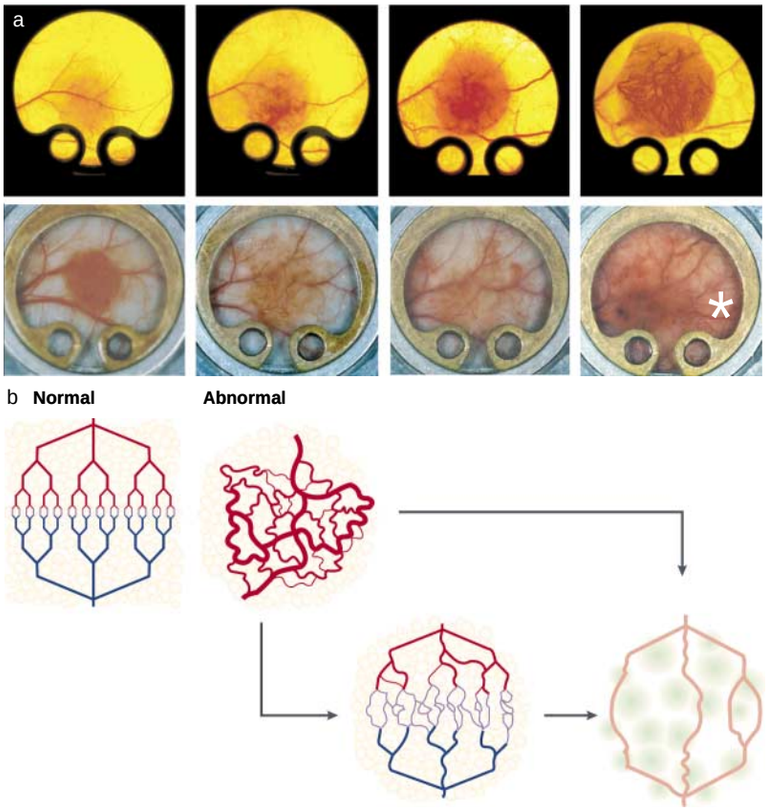

Figure 6 | **Imaging therapeutic responses. a** | Tumour growth in the dorsal window chamber over a 20-day period without (top) and with (bottom) therapy. In the treated animal, the tumour regresses, but then eventually escapes the therapy to re-grow (*). **b** | Tumour vessels, which are abnormally tortuous with chaotic branching patterns, can pass through a phase of 'normalization' during anti-angiogenic therapy. This can help in delivering drugs more efficiently to the tumour cells; if the blood supply becomes inadequate, drug delivery will be impaired. Part **a** (top) reproduced with permission from REF. 66 © (1992) American Association for Cancer Research; part **a** (bottom) reproduced with permission from REF. 45 © (1998) National Academy of Sciences USA; part **b** reproduced with permission from REF. 84 © (2001) Macmillan Magazines Ltd.

Virtually all IVM studies have used transplanted tumours. In principle, it should be possible to place 'windows' on spontaneously occurring tumours, but this has not yet been done. Alternatively, mice could be engineered with tissue-specific promoters so that tumours spontaneously arise in regions in which the windows summarized in TABLE 1 can be used.

Various molecular probes are available for anatomical and functional imaging. However, there are few probes for molecular imaging. GFP and its variants have already allowed visualization of molecular processes that, until recently, could only be imagined. However, these live reporters can be toxic[92] and show significant spectral overlap[93,94]. This might limit the number of reporters that can be used simultaneously[95]. However, the rapid developments that are taking place in this area are likely to overcome these problems[14,15,22–24,96]. For example, mathematical modelling of the emission spectra of multiple GFP variants can now be used to separate the contribution of each individual probe[97]. Live reporters are needed to dissect protein–protein interactions and to investigate signal-transduction pathways *in vivo*. Unexpected discoveries might emerge when we can examine the interaction of multiple genes in an intact organism using new molecular probes.

Concerted efforts are also needed to improve subsurface imaging technologies. Most of the current data come from techniques that emphasize surface features at the expense of information that is found from deeper within the tissue. Multi-photon laser-scanning microscopy can image structures up to 700 μm deep, depending on the tissues and probes used[3,98,99]. Other optical techniques, such as optical coherence tomography, can image deeper regions[100,101], but its application to intravital microscopy has been limited owing to lack of intrinsic contrast[102,103]. An alternative approach is fluorescence-mediated tomography[12]. Other techniques such as positron-emission tomography, computed tomography, magnetic resonance imaging and near-infrared imaging have been developed for use in rodent models and can provide deeper imaging, but they lack spatial resolution[12].

Image acquisition rate and speed of imaging also need to be improved. High-speed imaging is necessary to capture dynamic events such as blood flow, leukocyte–endothelial interactions, tumour-cell–blood-vessel interactions and movement of small molecules[4]. Such kinetic information is vital for understanding the biology of tumours and for optimizing therapeutic approaches.

Most IVM set-ups are bulky bench-top devices, but there is an increasing effort to miniaturize the cameras and microscopes to make the whole unit hand-held[104,105]. The prototypes of these microscopes have already proven useful for anatomical and molecular imaging of blood vessels, nerves, glands, calcium transients, and reporter-gene expression in brain, skin and colon, which are optically accessible with minimum invasion in experimental settings. Furthermore, these prototypes were able to detect subsurface changes associated with disease such as thermal injury and ulcerative colitis. As these devices become more user-friendly, IVM will become a useful clinical tool for diagnosis and monitoring the response of cancer patients to various therapies.

1. Jain, R. K., Schlenger, K., Hockel, M. & Yuan, F. Quantitative angiogenesis assays: progress and problems. *Nature Med.* **3**, 1203–1208 (1997).
2. Jain, R. K., Munn, L. L. & Fukumura, D. in *Tumor Models in Cancer Research* (ed. Teicher, B. A.) 647–671 (Humana, Totowa, 2001).
3. Brown, E. B. *et al. In vivo* measurement of gene expression, angiogenesis, and physiological function in tumors using multiphoton laser scanning microscopy. *Nature Med.* **7**, 864–868 (2001).
First and comprehensive application of multi-photon laser-scanning microscopy for molecular, cellular, anatomical and functional imaging of tumors *in vivo*.
4. Padera, T. P., Stoll, B. R., So, P. T. C. & Jain, R. K. High-speed intravital multiphoton laser scanning microscopy of microvasculature, lymphatics, and leukocyte-endothelial interactions. *Mol. Imaging* **1**, 9–15 (2002).
High-speed image acquisition by multi-photon laser-scanning microscopy for intravital microscopy.
5. Nugent, L. J. & Jain, R. K. Extravascular diffusion in normal and neoplastic tissues. *Cancer Res.* **44**, 238–244 (1984).
6. Yuan, F. *et al.* Vascular permeability and microcirculation of gliomas and mammary carcinomas transplanted in rat and mouse cranial window. *Cancer Res.* **54**, 4564–4568 (1994).
Establishment of cranial window models. Revealed intra- and inter-tumour heterogeneity of vascular permeability.
7. Jain, R. K. Barriers to drug delivery in solid tumors. *Sci. Am.* **271**, 58–65 (1994).

8. Martin, G. R. & Jain, R. K. Noninvasive measurement of interstitial pH profiles in normal and neoplastic tissue using fluorescence ratio imaging microscopy. *Cancer Res.* **54**, 5670–5674 (1994).
9. Torres-Filho, I. P., Leunig, M., Yuan, F., Intaglietta, M. & Jain, R. K. Noninvasive measurement of microvascular and interstitial oxygen profiles in a human tumor in SCID mice. *Proc. Natl Acad. Sci. USA* **91**, 2081–2085 (1994).
10. Helmlinger, G., Yuan, F., Dellian, M. & Jain, R. K. Interstitial pH and pO_2 gradients in solid tumors *in vivo*: high-resolution measurements reveal a lack of correlation. *Nature Med.* **3**, 177–182 (1997).
First high spatial-resolution dual measurements of tumour pH and pO_2. Revealed lack of correlation between tissue pH and pO_2 in solid tumours.
11. Fukumura, D. *et al.* Hypoxia and acidosis independently up-regulate vascular endothelial growth factor transcription in brain tumors *in vivo*. *Cancer Res.* **61**, 6020–6024 (2001).
First simultaneous measurement of gene promoter activity and microenvironmental parameters. Revealed regulation of VEGF by tissue pO_2 and pH by distinct pathways.
12. Weissleder, R. Scaling down imaging: molecular mapping of cancer in mice. *Nature Rev. Cancer* **2**, 11–18 (2002).
13. Becker, A. *et al.* Receptor-targeted optical imaging of tumors with near-infrared fluorescent ligands. *Nature Biotechnol.* **19**, 327–331 (2001).
14. Zhang, J., Ma, Y., Taylor, S. S. & Tsien, R. Y. Genetically encoded reporters of protein kinase A activity reveal impact of substrate tethering. *Proc. Natl Acad. Sci. USA* **98**, 14997–15002 (2001).
15. Ting, A. Y., Kain, K. H., Klemke, R. L. & Tsien, R. Y. Genetically encoded fluorescent reporters of protein tyrosine kinase activities in living cells. *Proc, Natl Acad. Sci. USA* **98**, 15003–15008 (2001).
References 14 and 15 are good examples of recent advances in molecular imaging probes. These are fusion protein reporters in which CFP and YFP are attached to a specific kinase-binding domain. Once the signalling pathway of interest is activated, the reporter fusion protein changes conformation and alters its fluorescence emission owing to fluorescence resonance energy transfer. By using ratio imaging, these probes allow quantitation of cellular level response/signalling.
16. Fukumura, D. *et al.* Tumor induction of VEGF promoter in stromal cells. *Cell* **94**, 715–725 (1998).
First *in vivo* visualization of gene promoter activity. Revealed VEGF activation in host stromal cells by tumour cells and underscored the importance of host–tumour interactions.
17. Tsuzuki, Y. *et al.* Vascular endothelial growth factor (VEGF) modulation by targeting hypoxia inducible factor-1α hypoxia response element VEGF cascade differentially regulates vascular response and growth rate in tumors. *Cancer Res.* **60**, 6248–6252 (2000).
18. Gohongi, T. *et al.* Tumor–host interactions in the gallbladder suppress distal angiogenesis and tumor growth: involvement of transforming growth factor-β1. *Nature Med.* **5**, 1203–1208 (1999).
19. Gullino, P. in *Cancer* (ed. Becker, F.) 327–354 (Plenum, New York, 1975).
20. Fidler, I. Seed and soil revisited: contribution of the organ microenvironment to cancer metastasis. *Surg. Oncol. Clin. N. Am.* **10**, 257–269 (2001).
21. Greer, L. & Szalay, A. Imaging of light emission from the expression of luciferase in living cells and organisms: a review. *Luminescence* **17**, 43–74 (2002).
22. Terskikh, A. *et al.* 'Fluorescent timer': protein that changes color with time. *Science* **290**, 1585–1588 (2000).
23. Baird, G. S., Zacharias, D. A. & Tsien, R. Y. Biochemistry, mutagenesis, and oligomerization of DsRed, a red fluorescent protein from coral. *Proc. Natl Acad. Sci. USA* **97**, 11984–11989 (2000).
24. Marchant, J. S *et al.* Multiphoton-evoked color change of DsRed as an optical highlighter for cellular and subcellular labeling. *Nature Biotechnol.* **19**, 645–649 (2001).
25. Wood, S. Pathogenesis of metastasis formation observed *in vivo* in the rabbit ear chamber. *Arch. Pathol.* **66**, 550–568 (1958).
26. Zeidman, I. The fate of circulating tumor cells. 1. Passage of cells through capillaries. *Cancer Res.* **21**, 38–39 (1961).
27. Chambers, A. F. *et al.* Steps in tumor metastasis: new concepts from intravital videomicroscopy. *Cancer Metastasis Rev.* **14**, 279–301 (1995).
28. Li, C.-Y. *et al.* Initial stages of tumor cell-induced angiogenesis: evaluation via skin window chambers in rodent models. *J. Natl Cancer Inst.* **92**, 143–147 (2000).
29. Chang, Y. S. *et al.* Mosaic blood vessels in tumors: frequency of cancer cells in contact with flowing blood. *Proc. Natl Acad. Sci USA* **97**, 14608–14613 (2000).
30. Wyckoff, J. B., Jones, J. G., Condeelis, J. S. & Segall, J. E. A critical step in metastasis: *in vivo* analysis of intravasation at the primary tumor. *Cancer Res.* **60**, 2504–2511 (2000).
31. Chishima, T. *et al.* Cancer invasion and micrometastasis visulaized in live tissue by green fluorescent protein expression. *Cancer Res.* **57**, 2042–2047 (1997).
32. Naumov, G. N. *et al.* Cellular expression of green fluorescent protein, coupled with high-resolution *in vivo* videomicroscopy, to monitor steps in tumor metastasis. *J. Cell Sci.* **112**, 1835–1842 (1999).
References 27–32 are representative studies using GFP-labelled cells to understand various steps in metastasis.
33. Jain, R. K. & Fenton, B. T. Intra-tumor lymphatic vessels: a case of mistaken identity or malfunction. *J. Natl Cancer Instit.* **94**, 417–421 (2002).
34. Ohkubo, C., Bigos, D. & Jain, R. K. Interleukin 2 induced leukocyte adhesion to the normal and tumor microvascular endothelium *in vivo* and its inhibition by dextran sulfate: implications for vascular leak syndrome. *Cancer Res.* **51**, 1561–1563 (1991).
35. Wu, N. Z., Klitzman, B., Dodge, R. & Dewhirst, M. W. Diminished leukocyte–endothelium interaction in tumor microvessels. *Cancer Res.* **52**, 4265–4268 (1992).
36. Fukumura, D. *et al.* Tumor necrosis factor-α-induced leukocyte adhesion in normal and tumor vessels: effect of tumor type, transplantation site, and host strain. *Cancer Res.* **55**, 4824–4829 (1995).
References 34–36 are representative works that show heterogeneous leukocyte–endothelium interactions in tumours.
37. Jain, R. K. *et al.* Leukocyte–endothelial adhesion and angiogenesis in tumors. *Cancer Metastasis Rev.* **15**, 195–204 (1996).
38. Fukumura, D., Yuan, F., Endo, M. & Jain, R. K. Role of nitric oxide in tumor microcirculation: blood flow, vascular permeability, and leukocyte–endothelial interactions. *Am. J. Pathol.* **150**, 713–725 (1997).
39. Fukumura, D., Yuan, F., Monsky, W. L., Chen, Y. & Jain, R. K. Effect of host microenvironment on the microcirculation of human colon adenocarcinoma. *Am. J. Pathol.* **151**, 679–688 (1997).
40. Jain, R. K., Munn, L. L., Fukumura, D. & Melder, R. J. in *Methods in Molecular Medicine Vol. 18: Tissue Engineering Methods and Protocols* (eds Morgan, J. R. & Yarmush, M. L.) 553–575 (Humana, Totowa, 1998).
41. Sasaki, A., Melder, R. J., Whiteside, T. L., Herberman, R. B. & Jain, R. K. Preferential localization of human adherent lymphokine-activated killer cells in tumor microcirculation. *J. Natl Cancer Inst.* **83**, 433–437 (1991).
42. Melder, R. J., Salehi, H. A. & Jain, R. K. Interaction of activated natural killer cells with normal and tumor vessels in cranial windows in mice. *Microvascular Res.* **50**, 35–44 (1995).
43. Melder, R. J. *et al.* During angiogenesis, vascular endothelial growth factor and basic fibroblast growth factor regulate natural killer cell adhesion to tumor endothelium. *Nature Med.* **2**, 992–997 (1996).
44. Detmar, M. *et al.* Increased microvascular density and enhanced leukocyte rolling and adhesion in the skin of VEGF transgenic mice. *J. Invest. Dermatol.* **111**, 1–6 (1998).
45. Jain, R. K. *et al.* Endothelial cell death, angiogenesis, and microvascular function after castration in an androgen-dependent tumor: role of vascular endothelial growth factor. *Proc. Natl Acad. Sci. USA* **95**, 10820–10825 (1998).
First demonstration of 'normalization' of tumour vasculature in response to anti-angiogenic treatment.
46. Kadambi, A. *et al.* Vascular endothelial growth factor (VEGF)-C differentially affects tumor vascular function and leukocyte recruitment: role of VEGF-receptor 2 and host VEGF-A. *Cancer Res.* **61**, 2404–2408 (2001).
47. Melder, R. J., Yuan, J., Munn, L. L. & Jain, R. K. Erythrocytes enhance lymphocyte rolling and arrest *in vivo*. *Microvascular Res.* **59**, 316–322 (2000).
48. Yamada, S., Melder, R. J., Leunig, M., Ohkubo, C. & Jain, R. K. Leukocyte rolling increases with age. *Blood* **86**, 4707–4708 (1995).
49. Yu, J. L. *et al.* Heterogeneous vascular dependence of tumor cell populations. *Am. J. Pathol.* **158**, 1325–1334 (2001).
50. Groner, W. *et al.* Orthogonal polarization spectral imaging: a new method for study of the microcirculation. *Nature Med.* **5**, 1209–1213 (1999).
51. Yuan, F. *et al.* Microvascular permeability and interstitial penetration of sterically stabilized (stealth) liposomes in a human tumor xenograft. *Cancer Res.* **54**, 3352–3356 (1994).
52. Yuan, F. *et al.* Time-dependent vascular regression and permeability changes in established human tumor xenografts induced by an anti-vascular endothelial growth factor/vascular permeability factor antibody. *Proc. Natl Acad. Sci. USA* **93**, 14765–14770 (1996).
53. Endrich, B., Reinhold, H. S., Gross, J. F. & Intaglietta, M. Tissue perfusion inhomogeneity during early tumor growth in rats. *J. Natl Cancer Inst.* **62**, 387–395 (1979).
54. Endrich, B., Intaglietta, M., Reinhold, H. S. & Gross, J. F. Hemodynamic characteristics in microcirculatory blood channels during early tumor growth. *Cancer Res.* **39**, 17–23 (1979).
References 53 and 54 described, for the first time, the use of IVM to measure temporal and spatial heterogeneity in tumour blood flow.
55. Jain, R. K. Determinants of tumor blood flow: a review. *Cancer Res.* **48**, 2641–2658 (1988).
56. Gazit, Y., Berk, D. A., Leunig, M., Baxter, L. T. & Jain, R. K. Scale-invariant behavior and vascular network formation in normal and tumor tissue. *Phys. Rev. Lett.* **75**, 2428–2431 (1995).
57. Baish, J. W. & Jain, R. K. Fractals and cancer. *Cancer Res.* **60**, 3683–3688 (2000).
58. Izumi, Y., Xu, L., diTomaso, E., Fukumura, D. & Jain, R. K. Herceptin acts as an anti-angiogenic cocktail. *Nature* **416**, 279–280 (2002).
59. Leu, A. J., Berk, D. A., Lymboussaki, A., Alitalo, K. & Jain, R. K. Absence of functional lymphatics within a murine sarcoma: a molecular and functional evaluation. *Cancer Res.* **60**, 4324–4327 (2000).
60. Padera, T. P., Yun, C.-O., Carreira, C. M. & Jain, R. K. Local mechanics and VEGF-C alter peri-tumor lymphatic function. *Proc. Am. Assoc. Cancer Res.* **41**, 88 (2000).
References 59 and 60 show the lack of functional lymphatics within tumours and lymphatic hyperplasia in the tumour margin.
61. Jeltsch, M. *et al.* Hyperplasia of lymphatic vessels in VEGF-C transgenic mice. *Science* **276**, 1423–1425 (1997).
62. Hobbs, S. K. *et al.* Regulation of transport pathways in tumor vessels: role of tumor type and host microenvironment. *Proc. Natl Acad. Sci. USA* **95**, 4607–4612 (1998).
First determination of pore size in tumour vessels and how pore size is affected by host–tumour interactions and the microenvironment.
63. Monsky, W. L. *et al.* Augmentation of transvascular transport of macromolecules and nanoparticles in tumors using vascular endothelial growth factor. *Cancer Res.* **59**, 4129–4135 (1999).
64. Hashizume, H. *et al.* Openings between defective endothelial cells explain tumor vessel leakiness. *Am. J. Pathol.* **156**, 1363–1380 (2000).
65. Jain, R. K. Delivery of molecular medicine to solid tumors: lessons from *in vivo* imaging of gene expression and function. *J. Controlled Release* **74**, 7–25 (2001).
66. Leunig, M. *et al.* Angiogenesis, microvascular architecture, microhemodynamics, and interstitial fluid pressure during early growth of human adenocarcinoma LS174T in SCID mice. *Cancer Res.* **52**, 6553–6560 (1992).
67. Carmeliet, P. & Jain, R. K. Angiogenesis in cancer and other diseases: from genes to function to therapy. *Nature* **407**, 249–257 (2000).
68. Gerlowski, L. E. & Jain, R. K. Microvascular permeability of normal and neoplastic tissues. *Microvasc. Res.* **31**, 288–305 (1986).
69. Yuan, F., Leunig, M., Berk, D. A. & Jain, R. K. Microvascular permeability of albumin, vascular surface area, and vascular volume measured in human adenocarcinoma LS174T using dorsal chamber in SCID mice. *Microvasc. Res.* **45**, 269–289 (1993).
70. Lichtenbeld, H. C., Yuan, F., Michel, C. C. & Jain, R. K. Perfusion of single tumor microvessels: application to vascular permeability measurement. *Microcirculation* **3**, 349–357 (1996).
References 68–70 describe vascular permeability measurements in tumour vessels and demonstrate the lack of convection.
71. Jain, R. K. & Munn, L. L. Leaky vessels? Call Ang1! *Nature Med.* **6**, 131–132 (2000).
72. Yuan, F. *et al.* Vascular permeability in a human tumor xenograft: molecular size dependence and cut-off size. *Cancer Res.* **55**, 3752–3756 (1995).
73. Dellian, M., Yuan, F., Trubetskoy, V., Torchilin, V. & Jain, R. K. Vascular permeability in a human tumor xenograft: molecular charge dependence. *Br. J. Cancer* **82**, 1513–1518 (2000).
74. Thurston, G. *et al.* Cationic liposomes target angiogenic endothelial cells in tumors and chronic inflammation in mice. *J. Clin. Invest.* **101**, 1401–1413 (1998).

75. Chary, S. R. & Jain, R. K. Direct measurement of interstitial convection and diffusion of albumin in normal and neoplastic tissues by fluorescence photobleaching. *Proc. Natl Acad. Sci. USA* **86**, 5385–5389 (1989).
76. Berk, D. A., Yuan, F., Leunig, M. & Jain, R. K. Direct *in vivo* measurement of targeted binding in a human tumor xenograft. *Proc. Natl Acad. Sci. USA* **94**, 1785–1790 (1997).
References 75 and 76 provided the first measurements of convection, diffusion and binding of molecules *in vivo*.
77. Netti, P. A., Berk, D. A., Swartz, M. A., Grodzinsky, A. J. & Jain, R. K. Role of extracellular matrix assembly in interstitial transport in solid tumors. *Cancer Res.* **60**, 2497–2503 (2000).
78. Pluen, A. *et al.* Role of tumor–host interactions in interstitial diffusion of macromolecules: cranial vs. subcutaneous tumors. *Proc. Natl Acad. Sci. USA* **98**, 4628–4633 (2001).
79. Leu, A. J., Berk, D. A., Yuan, F. & Jain, R. K. Flow velocity in the superficial lymphatic network of the mouse tail. *Am. J. Physiol.* **267**, H1507–H1513 (1994).
80. Berk, D. A., Swartz, M. A., Leu, A. J. & Jain, R. K. Transport in lymphatic capillaries. II. Microscopic velocity measurement with fluorescence photobleaching. *Am. J. Physiol.* **270**, H330–H337 (1996).
81. Swartz, M. A., Berk, D. A. & Jain, R. K. Transport in lymphatic capillaries. I. Macroscopic measurements using residence time distribution theory. *Am. J. Physiol.* **270**, H324–H329 (1996).
82. Lee, C. G. *et al.* Anti-vascular endothelial growth factor treatment augments tumor radiation response under normoxic or hypoxic conditions. *Cancer Res.* **60**, 5565–5570 (2000).
83. Hansen-Algenstaedt, N. *et al.* Tumor oxygenation in hormone-dependent tumors during vascular endothelial growth factor receptor-2 blockade, hormone ablation, and chemotherapy. *Cancer Res.* **60**, 4556–4560 (2000).
84. Jain, R. K. Normalizing tumor vaculature with anti-angiogenic therapy: a new paradigm for combination therapy. *Nature Med.* **7**, 987–989 (2001).
85. Teicher, B. A. *et al.* Potentiation of cytotoxic therapies by TNP-470 and minocycline in mice bearing EMT-6 mammary carcinoma. *Breast Cancer Res. Treat.* **36**, 227–236 (1995).
86. Browder, T. *et al.* Antiangiogenic scheduling of chemotherapy improves efficacy against experimental drug-resistant cancer. *Cancer Res.* **60**, 1878–1886 (2000).
87. Murata, R., Nishimura, Y. & Hiraoka, M. An antiangiogenic agent (TNP-470) inhibited reoxygenation during fractionated radiotherapy of murine mammary carcinoma. *Int. J. Radiat. Oncol. Biol. Phys.* **37**, 1107–1113 (1997).
88. Ma, J. *et al.* Pharmacodynamic-mediated reduction of temozolomide tumor concentrations by the angiogenesis inhibitor TNP-470. *Cancer Res.* **61**, 5491–5498 (2001).
89. Huang, Q. *et al.* Noninvasive visualization of tumors in rodent dorsal skin window chambers: a novel model for evaluating anti-cancer therapies. *Nature Biotechnol.* **17**, 1033–1035 (1999).
90. Vajkoczy, P., Ullrich, A. & Menger, M. Intravital fluorescence videomicroscopy to study tumor angiogenesis and microcirculation. *Neoplasia* **2**, 53–61 (2000).
91. Hoffman, R. M. Visualization of GFP-expressing tumors and metastasis *in vivo*. *BioTechniques* **30**, 1016–1026 (2001).
92. Huang, W. H., Aramburu, J., Douglas, P. S. & Izumo, S. Transgenic expression of green fluorescence protein can cause dilated cardiomyopathy. *Nature Med.* **6**, 482–483 (2000).
93. Garcia-Parajo, M. F., Koopman, M., van Dijk, E. M. H. P., Subramaniam, V. & van Hulst, N. F. The nature of fluorescence emission in the red fluorescent protein DsRed, revealed by single-molecule detection. *Proc. Natl Acad. Sci. USA* **98**, 14392–14397 (2001).
94. Cotlet, M. *et al.* Identification of different emitting species in the red fluorescent protein DsRed by means of ensemble and single-molecule spectroscopy. *Proc. Natl Acad. Sci. USA* **98**, 14398–14403 (2001).
95. Hadjantonakis, A. K. & Nagy, A. The color of mice: in the light of GFP-variant reporters. *Histochem. Cell Biol.* **115**, 49–58 (2001).
96. Mitchell, P. Turning the spotlight on cellular imaging. *Nature Biotechnol.* **19**, 1013–1017 (2001).
97. Roessel, P. V. & Brand, A. H. Imaging into the future: visualizing gene expression and protein interactions with fluorescent proteins. *Nature Cell Biol.* **4**, E15–E20 (2002).
98. Kleinfeld, D., Mitra, P. P., Helmchen, F. & Denk, W. Fluctuations and stimulus-induced changes in blood flow observed in individual capillaries in layers 2 through 4 of rat neocortex. *Proc. Natl Acad. Sci. USA* **95**, 15741–15746 (1998).
99. Lendvai, B., Stern, E. A., Chen, B. & Svoboda, K. Experience-dependent plasticity of dendritic spines in the developing rat barrel cortex *in vivo*. *Nature* **404**, 876–881 (2000).
100. Huang, D. *et al.* Optical coherence tomography. *Science* **254**, 1178–1181 (1991).
101. Boppart, S. *et al.* High resolution optical coherence tomography-guided laser ablation of surgical tissue. *J. Surg. Res.* **82**, 275–284 (1999).
102. Boppart, S. *et al. In vivo* cellular optical coherence tomography imaging. *Nature Med.* **4**, 861–865 (1998).
103. Beaurepaire, E., Moreaux, L., Amblard, F. & Mertz, J. Combined scanning optical coherence and two-photon excited fluorescence microscopy. *Optics Lett.* **24**, 969 (1999).
104. Delaney, P. M., Harris, M. R. & King, R. G. Novel microscopy using fibre optic confocal imaging and its suitability for subsurface blood vessel imaging *in vivo*. *Clin. Exp. Pharmacol. Physiol.* **20**, 197–198 (1993).
105. Helmchen, F., Fee, M. S., Tank, D. W. & Denk, W. A miniature head-mounted two-photon microscope: high-resolution brain imaging in freely moving animals. *Neuron* **31**, 903–912 (2001).
Development of a miniature two-photon microscope.
106. Shioda, T., Munn, L., Fenner, M., Jain, R. & Isselbacher, K. Early events of metastasis in the microcirculation involve changes in gene expression of cancer cells: tracking mRNA levels of metastasizing cancer cells in the chick embryo chorioallantoic membrane. *Am. J. Pathol.* **150**, 2099–2112 (1997).
107. Jain, R. K. Delivery of molecular and cellular medicine to solid tumors. *Microcirculation* **4**, 1–23 (1997).
108. Ide, A. G., Baker, N. H. & Warren, S. L. Vascularization of the Brown–Pearce rabbit epithelioma transplant as seen in the transparent ear chamber. *Am. J. Roentgenol.* **42**, 891–899 (1939).
109. Dudar, T. E. & Jain, R. K. Differential response of normal and tumor microcirculation to hyperthermia. *Cancer Res.* **44**, 605–612 (1984).
110. Algire, G. H. An adaptation of the transparent chamber technique to the mouse. *J. Natl Cancer Inst.* **4**, 1–11 (1943).
111. Algire, G. H. Microscopic studies of the early growth of a transplantable melanoma of the mouse, using the transparent-chamber technique. *J. Natl Cancer Inst.* **4**, 13–20 (1943).
112. Kligerman, M. M. & Henel, D. K. Some aspects of the microcirculation of a transplantable experimental tumor. *Radiology* **76**, 810–817 (1961).
113. Reinhold, H. S. Improved microcirculation in irradiated tumours. *Eur. J. Cancer* **7**, 273–280 (1971).
114. Falkvoll, K. H., Rofstad, E. K., Brustad, T. & Marton, P. A transparent chamber for the dorsal skin fold of athymic mice. *Exp. Cell Biol.* **52**, 260–268 (1984).
115. Asaishi, K., Endrich, B., Gotz, A. & Messmer, K. Quantitative analysis of microvascular structure and function in the amelanotic melanoma A-Mel-3. *Cancer Res.* **41**, 1898–1904 (1981).
116. Yamura, H., Suzuki, M. & Sato, H. Transparent chamber in the rat skin for studies on microcirculation in cancer tissue. *Gann* **62**, 177–185 (1971).
117. Reinhold, H. S., Blachiwiecz, B. & Blok, A. Oxygenation and reoxygenation in 'Sandwich' tumours. *Bibl. Anat.* **15**, 270–272 (1977).
118. Dewhirst, M. W. *et al.* Morphologic and hemodynamic comparison of tumor and healing normal tissue microvasculature. *Int. J. Radiat. Oncol. Biol. Phys.* **17**, 91–99 (1989).
119. Lutz, B. R., Fulton, G. P., Patt, D. I. & Handler, A. H. The growth rate of tumor transplants in the cheek pouch of the hamster (*Mesocricetus auratus*). *Cancer Res.* **10**, 231–232 (1950).
120. Chute, R. N., Sommers, S. C. & Warren, S. Hetero-transplantation of human cancer. II. Hamster cheek pouch. *Cancer Res.* **12**, 912–914 (1952).
121. Toolan, H. W. Transplantable human neoplasms maintained in cortisone-treated laboratory animals: H. S. #1; H. Ep. #1; H. Ep. # 2; H. Ep. # 3; and H. Emb. Rh. #1. *Cancer Res* **14**, 660–666 (1954).
122. Goodall, C. M., Sanders, A. G. & Shubik, P. Studies of vascular patterns in living tumors with a transparent chamber inserted in hamster cheek pouch. *J. Natl Cancer Inst.* **35**, 497–521 (1965).
123. Eddy, H. A. & Casarett, G. W. Development of the vascular system in the hamster malignant neurilemmoma. *Microvasc. Res.* **6**, 63–82 (1973).
124. Norrby, K., Jakobsson, A. & Sörbo, J. Quantitative angiogenesis in spreads of intact rat mesenteric windows. *Microvasc. Res.* **39**, 341–348 (1990).
125. Yanagi, K. & Ohsima, N. Angiogenic vascular growth in the rat peritoneal disseminated tumor model. *Microvasc. Res.* **51**, 15–28 (1996).
126. Heuser, L. S. & Miller, F. N. Differential macromolecular leakage from the vasculature of tumors. *Cancer* **57**, 461–464 (1986).
127. Monsky, W. L. *et al.* Role of host microenvironment in angiogenesis and microvascular functions in human breast cancer xenografts: mammary fat pad vs. cranial tumors. *Clin. Cancer Res* **8**, 1008–1013 (2002)
128. Schmidt, J. *et al.* Reduced basal and stimulated leukocyte adherence in tumor endothelium of experimental pancreatic cancer. *Int. J. Pancreatol.* **26**, 173–179 (1999).
129. Tsuzuki, Y. *et al.* Pancreas microenvironment promotes VEGF expression and tumor growth: novel window models for pancreatic tumor angiogenesis and microcirculation. *Lab. Invest.* **81**, 1439–1452 (2001).
130. Funakoshi, N. *et al.* A new model of lung metastasis for intravital studies. *Microvasc. Res.* **59**, 361–367 (2000).
131. Luckè, B. & Schlumberger, H. The manner of growth of frog carcinoma, studied by direct microscopic examination of living intraocular transplants. *J. Exp. Med.* **70**, 257–268 (1939).
132. Greene, H. S. N. The significance of heterologous transplantability of human cancer. *Cancer* **5**, 24–44 (1952).
133. Gimbrone, M. A. J. & Gullino, P. M. Angiogenic capacity of preneoplastic lesions of the murine mammary gland as a marker of neoplastic transformation. *Cancer Res.* **36**, 2611–2620 (1976).
134. Brem, S. S., Gullino, P. M. & Medina, D. Angiogenesis: a marker for neoplastic transformation of mammary papillary hyperplasia. *Science* **195**, 880–882 (1977).
135. Maiorana, A. & Gullino, P. M. Acquisition of angiogenic capacity and neoplastic transformation in the rat mammary gland. *Cancer Res.* **38**, 4409–4414 (1978).
136. Gimbrone, M. A. J., Cotran, R. S., Leapman, S. B. & Folkman, J. Tumor growth and neovascularization: an experimental model using the rabbit cornea. *J. Natl Cancer Inst.* **52**, 413–427 (1974).
137. Ausprunk, D. H. & Folkman, J. Migration and proliferation of endothelial cells in preformed and newly formed blood vessels during tumor angiogenesis. *Microvasc. Res.* **14**, 53–65 (1977).
138. Muthukkaruppan, V. R. & Auerbach, R. Angiogenesis in the mouse cornea. *Science* **205**, 1416–1418 (1979).
139. Suit, H. & Shalek, R. Response of anoxic C3H mouse mammary carcinoma isotransplants (I-25mm3) to X-irradiation. *J. Natl Cancer Inst.* **31**, 479–495 (1963).
140. Dellian, M., Witwer, B. P., Salehi, H. A., Yuan, F. & Jain, R. K. Quantitation and physiological characterization of angiogenic vessels in mice: effect of basic fibroblast growth factor, vascular endothelial growth factor/vascular permeability factor, and host microenvironment. *Am. J. Pathol.* **149**, 59–72 (1996).
141. Dewhirst, M. *et al.* Quantification of longitudinal tissue pO_2 gradients in window chamber tumours: impact on tumor hypoxia. *Br. J. Cancer* **79**, 1717–1722 (1999).
142. Kimura, H. *et al.* Fluctuations in red cell flux in tumor microvessels can lead to transient hyoxia and reoxygenation in tumor parenchyma. *Cancer Res.* **56**, 5522–5528 (1996).

Acknowledgements

We thank E. Brown, M. Dewhirst, M. Intaglietta, B. Seed, P. So and R. Weissleder for their helpful comments. This work was supported by National Institute of Health grants.

Online links

DATABASES

The following terms in this article are linked online to:

LocusLink: http://www.ncbi.nlm.nih.gov/LocusLink/

bFGF | cathepsin B | CD31 | CD105 | ERBB2 | E-selectin | HIF1α | ICAM1 | PlGF | TNF-α | VCAM1 | VEGF | VEGFC | VEGFR1 | VEGFR2

Medscape DrugInfo:

http://promini.medscape.com/drugdb/search.asp

adriamycin | Herceptin

FURTHER INFORMATION

Edwin L. Steele Laboratory: http://steele.mgh.harvard.edu

Access to this interactive links box is free online.